JCIM JOURNAL OF CHEMICAL INFORMATION AND MODELING

pubs.acs.org/jcim Article

A Highly Efficient Neutral Anion Receptor in Polar Environments by Synergy of Anion−π Interactions and Hydrogen Bonding

Marta Queizán, Marta Sánchez-Lozano, Marcos Mandado, and Jose M. Hermida-Ramón*

Cite This: *J. Chem. Inf. Model.* 2021, 61, 4455−4461 Read Online

ACCESS | Metrics & More | Article Recommendations | Supporting Information

ABSTRACT: Herein, it is shown how anion recognition in highly polar solvents by neutral metal-free receptors is feasible when multiple hydrogen bonding and anion−π interactions are suitably combined. A neutral aromatic molecular tweezer functionalized with azo groups is shown to merge these two kinds of interactions in a unique system and its efficiency as an anion catcher in water is evaluated using first-principles quantum methods. Theoretical calculations unequivocally prove the high thermodynamic stability in water of a model anion, bromide, captured within the tweezer's cavity. Thus, static calculations indicate anion−tweezer interaction energies within the range of covalent or ionic bonds and stability constants in water of more than 10 orders of magnitude. First-principles molecular dynamics calculations also corroborate the stability through the time of the anion−tweezer complex in water. It shows that the anion is always found within the tweezer's cavity due to the combination of the tweezer−anion interactions plus a hydrogen bond between the anion and a water molecule that is inside the tweezer's cavity.

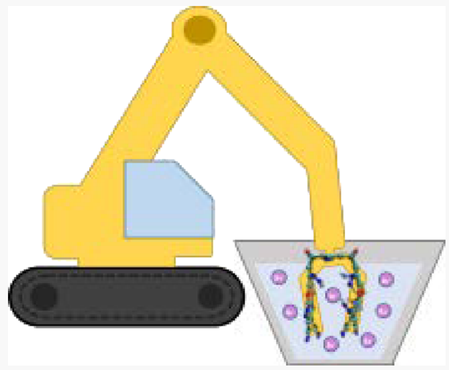

■ INTRODUCTION

Since the characterization of stabilizing anion−π interactions in the earliest 2000s,[1−4] a considerable amount of work has been carried out on this topic[5−14] due to the important role played by anions and anion receptors in chemical, biological, medical, and environmental processes.[15−19] Particularly, the anion−π interactions have attracted interest because they improve the selectivity and directionality of anion receptors,[9,12,13,19] providing tailor-made solutions for problems involving anions. Among the characteristics of this new family of receptors, the most important are the neutrality, the variety in size and shape of the target anions, and the wide range of stability produced by their interactions.[5,6]

Molecular tweezers and clips are ion receptors characterized by the presence of two flat pincers separated by a more or less rigid tether. They have the ability to form complexes with a substrate by gripping it between their tips in a similar manner to that of mechanical tweezers. Particularly interesting are Klärner's molecular tweezers.[20−23] They are characterized by a concave−convex topology and a negative molecular electrostatic potential in the concave region, which lends them the ability to bind electrodeficient aromatic and aliphatic substrates as well as organic cations.[22] Yet, the electrostatic potential within the tweezers' molecular cavity may be chemically controlled by means of aromatic ring substitutions, turning a cation receptor into an anion receptor.[24−27]

In this study, we present a new neutral molecular tweezer that combines anion−π and hydrogen bond interactions[28−31] in the process of anion trapping. Herein, the interplay between hydrogen and anion−π bonding leads to interaction energies comparable to covalent or ionic bonds. It is one of the very few examples of a stable complex formed by an anion captured within a neutral metal-free receptor in water.[19,30] However, stability constants as high as those obtained with this tweezer have never been reported before. Bromide has been chosen as the test anion due to its medium size and spherical shape, which simplifies the computational work. First, a static study has been performed in order to evaluate the energetics and the intermolecular forces involved in the process of anion recognition. Next, an additional first-principles molecular dynamics study in water has been performed to verify the stability of the tweezer−anion complex.

■ COMPUTATIONAL METHODS

The static calculations were carried out using two different computational levels. For once, the BLYP functional plus DFT-D3[32] empirical dispersion correction (BLYP-D3), the level subsequently used in the quantum molecular dynamics simulations, was employed in combination with the def2-SVP basis set. Since the BLYP functional alone poorly describes the dispersion interactions and def2-SVP is a rather small basis set, calculations were also performed with the

Received: May 26, 2021
Published: August 16, 2021

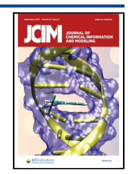

M062X-D3 functional and the 6-31++G(d,p) basis set. This functional was proven to account properly for medium-range dispersion[33] and requires a small empirical correction in the case of long-range interactions.[34] In addition, diffuse functions were included in the 6-31++G(d,p) basis set, which is highly recommended for the study of anions. The static calculations were performed using the Gaussian[35] and ORCA[36,37] packages.

Gas-phase binding and interaction energies, E_{bind} and E_{int}, were calculated with the supermolecular approach. The former is equal to the latter plus the energy associated with the deformation of the tweezer's geometry in the complex structure, E_{def}. An energy decomposition analysis (EDA) of the interaction energy based on deformation densities was additionally performed. Details about the theory behind the EDA applied in this study may be found elsewhere.[34,38] Herein, we will just mention that it enables the well-known partition of the total interaction energy into electrostatic, E_{elec}, Pauli repulsion, E_{Pau}, induction, E_{ind}, and dispersion, E_{disp}, energies. The electrostatic energy is obtained from the unperturbed electron densities of the fragments and their nucleus potentials and it is also known as the "classical" electrostatic energy. The Pauli repulsion contains two terms: one arising from the intermolecular electron exchange (stabilizing term) and another one arising from the intermolecular electron spin repulsion (destabilizing term). On the other hand, the induction energy is extracted from the polarization energy, the one stemming from the relaxation of the electron densities in the complex, by merging its definition given by the second-order perturbation theory into the corresponding EDA equations.[9] The rest of the polarization energy thus contains the second-order dispersion energy plus the energy components of third order and higher orders in the perturbation scheme although the dispersion energy is certainly the main contributor and therefore we denote this term here as E_{disp}. All the terms are naturally corrected for the basis set superposition error using the counterpoise method.[39]

A topological analysis of the electron density was performed using the quantum theory of atoms in molecules[40] for the tweezer−bromide equilibrium geometries obtained with the BLYP-D3/def2-SVP and M062X-D3/6-31++G(d,p) computational levels. Both the intramolecular and intermolecular bond critical points (BCPs) together with the corresponding bond paths were represented with AIM2000 software.[41]

A first-principles molecular dynamics simulation (MDS) of the tweezer−bromide complex together with 100 water molecules was carried out. The 3-21G basis set was used to describe the water molecules, and the tweezer−bromide complex was described by a def2-SVP basis set. All calculations were carried out with the BLYP functional and the DFT-D3 empirical correction to dispersion.[32] In order to perform the simulation, first we carried out optimization of the complete system to find a stationary point that will act as the starting point for the simulation. Then, a heating procedure up to a temperature of 300 K was carried out by performing a 100 fs simulation using a Berendsen thermostat[42] at a constant pressure of 1 atmosphere. Afterward, we performed equilibration of 2000 fs at 300 K in a 19.4 Å × 15.2 Å × 14.8 Å orthorhombic cell that matches the shape of the tweezer and keeps the density of the system at approximately 1 g·cm^{-3}. Finally, a production simulation of 11 ps in the mentioned orthorhombic cell at 300 K was carried out and the results were analyzed. The timestep used throughout the MDS was 0.5 fs. A harmonic repulsive potential was applied outside the cell to retain the molecules inside. This potential depends on the closest distance from the atom's center to the defined cell surface. The spring constant used in the harmonic potential was 10 kJ·mol^{-1}·Å^{-2}. All MD calculations were performed with the ORCA package.[36,37]

■ RESULTS AND DISCUSSION

The optimized structures of the tweezer−Br$^-$ complex and the isolated tweezer obtained with the BLYP-D3/def2-SVP and M062X-D3/6-31++G(d,p) levels of theory are shown in Figure 1. Frequencies and force constants were obtained, and

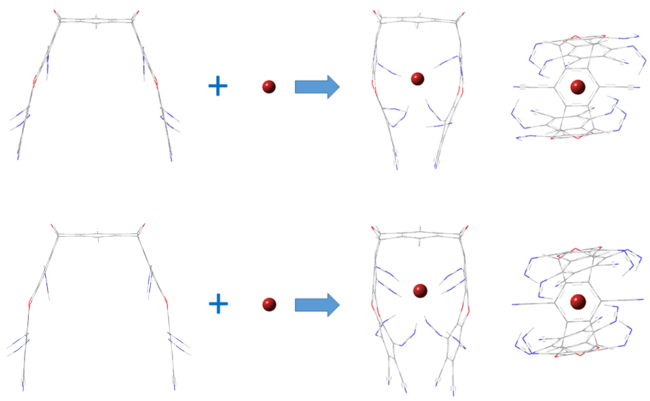

Figure 1. Isolated tweezer and tweezer−Br complex structures obtained with BLYP-D3 (top) and M062X-D3 (bottom) functionals.

all the conformations were characterized as energy minima (see Supporting Information). Two stable conformers were found for the isolated tweezer, displaying the tweezer's arms as a convex or concave disposition, respectively. The former was found to be slightly more stable than the latter by 3.2 and 1.2 kcal/mol using M062X-D3/6-31++G(d,p) and BLYP-D3/def2-SVP levels, respectively. This is the conformer shown in Figure 1, and the coordinates of the other conformer are provided in the Supporting Information. Even though the isolated tweezer's structure for both computational levels is quite similar, the difference in the deformation energy is remarkable, which is 9.65 kcal·mol^{-1} larger at the M062X-D3 level (see Table 1). This is due to the stronger interaction predicted by this functional, which comes also with a larger deformation of the tweezer's geometry in the complex.

The values obtained for the total interaction energy and its components are listed in Table 1. As can be observed, the interaction energies obtained with any of the two functionals are huge; however, M062X-D3 predicts a stronger attractive interaction (about 16 kcal·mol^{-1} higher). The lack of diffuse functions with the BLYP-D3 functional may lead to underestimated dispersion energies and less attractive interactions, as shown in previous studies.[43] However, this result is not general and the lack of diffuse functions may result in more attractive interactions, as is the case for chalcogen bonds.[44] In order to quantify the effect of diffuse functions on the investigated tweezer−Br$^-$ complex, we recalculated the interaction energy and the corresponding energy components using the M062X-D3/6-31G(d,p) level (see Table 1). The results indicate a decrease in the interaction energy from −97.26 to −91.52 kcal/mol when the diffuse functions are removed with the largest change corresponding to the dispersion energy, from −73.96 to −66.80 kcal/mol. By even including deformation energies, we can observe that combining anion−π forces and

https://doi.org/10.1021/acs.jcim.1c00595
J. Chem. Inf. Model. 2021, 61, 4455−4461

Table 1. Binding and Interaction Energies and Their Different Components for the Tweezer−Br$^-$ Complexes Obtained at the M062X-D3/6-31++G(d,p) and BLYP-D3/def2-SVP Levels[a]

	M062X-D3	BLYP-D3
E_{bind}	−80.32	−73.70
E_{def}	16.94	7.29
E_{int}	−97.26/−91.52[c]	−80.99
E_{elec}	−129.29/−130.38[c]	−128.66
E_{Pau}	108.43/110.57[c]	113.64
E_{ind}	−2.44/−4.92[c]	−9.42
E_{disp}	−73.96 (−0.44)[b]/−66.80[c]	−56.59 (−19.17)[b]
ΔG_c(gas)	−66.53	−61.10
ΔH_c	−80.86	−72.73
$-T\Delta S_c$	13.34	11.63
ΔG_c(wat)	−15.35	−20.07
ΔH_c	−79.27	−72.14
$-T\Delta S_c$	13.34	11.63
ΔG_{solv}	50.58	40.44

[a]Thermodynamic information: complex enthalpy, thermal entropy, and Gibbs energy in the gas phase and aqueous solution at 298.15 K. All data are expressed in kcal·mol^{-1}. [b]DFT-D3 dispersion correction using zero damping is shown in parenthesis. [c]Energies using the 6-31G(d,p) basis set (see text).

hydrogen bonds in this molecular tweezer results in binding energies of the trapped anion of the order of a covalent carbon−carbon bond (around 80 kcal·mol^{-1}).

An analysis of the role played by different intermolecular forces can be carried out using the data listed in Table 1. The important role played by the hydrogen bonds is reflected by the very large electrostatic energy, which is not compensated by the Pauli repulsion. Summation of both terms gives rise to a net stabilization of −21 kcal·mol^{-1} with M062X-D3 and −15 kcal·mol^{-1} with BLYP-D3. This difference may be understood in terms of the ratio between the azo groups directly interacting with bromide and those forming intramolecular hydrogen bonds. As can be seen in Figure 1, this ratio is 6/2 for M062X-D3 and 4/4 for BLYP-D3 complexes. A topological analysis of the electron density using Bader's theory[40] (see Figure 2) confirms the hydrogen bond interactions mentioned above.

The induction forces are significantly smaller than the electrostatic forces. Even though they are larger with the BLYP-D3 functional, they represent less than 12% of the total interaction energy (3% with M062X-D3). On the contrary, dispersion forces are very large (76 and 70% of the total in M062X and BLYP-D3, respectively), being of the order of the total interaction energy previously reported for a cyanide-functionalized tweezer.[25] As expected, the highest differences are found here, the dispersion energy being 17 kcal·mol^{-1} lower at the M062X-D3/6-31++G(d,p) level.

The most relevant result so far is that functionalization with an azo group enhances the complex interaction energy by more than 20 kcal·mol^{-1} with respect to the cyanide group.[25] As discussed above, this enhancement stems from the extra N−H···Br$^-$ hydrogen bonds. In order to perform a crude estimation of the weight of the hydrogen bonds in the total interaction energy, we have taken the geometry of the dimer obtained with the M062X-D3 functional and removed the tweezer's skeleton from it but keeping the −N═N−H substituents in the same position and saturating the nitrogen

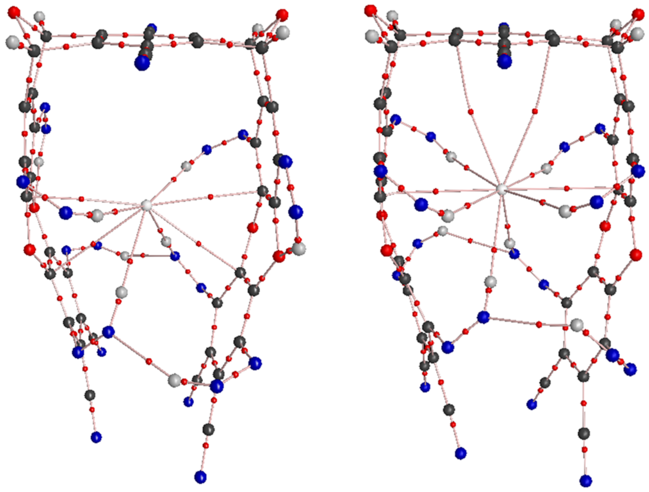

Figure 2. Intramolecular and intermolecular BCPs (small red circles) and the corresponding bond paths (white lines) obtained with the BLYP/def2-SVP (left) and M062X/6-31++G(d,p) (right) computational levels for the tweezer−Br$^-$ complex.

valence with a methyl group (Figure 3A). The interaction energy of this hypothetical system with the anion at the

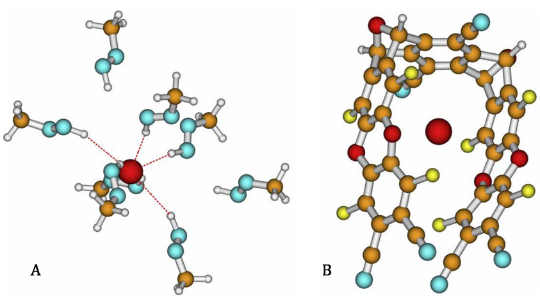

Figure 3. (A) System after removing the tweezer's skeleton. (B) System after replacing the −N═N−H substituents by fluorides (see text).

M062X-D3/6-31++G(d,p) level was −36.02 kcal/mol. This means that roughly one third of the interaction energy is due to the hydrogen bond. Also, since there are six hydrogen bonds, the stabilization of each hydrogen bond is around 6 kcal/mol. On the other hand, if the geometry of the dimer obtained with the M062X-D3 functional is taken and the −N═N−H substituents are replaced by fluorides to obtain a fluorinated tweezer (Figure 3B), the interaction energy with the anion is −56.80 kcal/mol. This energy added to that obtained for the hydrogen bonds becomes close to the total interaction energy of the dimer. The weight of the two energies with respect to the total interaction is rather similar when the same procedure is performed at the BLYP-D3/def2-SVP level. Thus, the energies are −28.14 kcal/mol for the hydrogen bonds and −50.20 kcal/mol for the interaction between the anion and the fluorinated tweezer.

The next step in this study is to explore whether this energy enhancement is sufficient to overcome the destabilizing thermal and solvation effects so that the complex is thermodynamically stable in the gas phase and aqueous solution. Therefore, we calculated the complexation enthalpy, thermal entropy, and free energy in both environments at a given temperature of 298.15 K. The solvation free energy was

https://doi.org/10.1021/acs.jcim.1c00595
J. Chem. Inf. Model. 2021, 61, 4455−4461

obtained with the continuum solvation model based on density.[45] The thermodynamic results are also included in Table 1. After the thermal corrections, the absolute value of the complexation enthalpy in the gas phase is much higher than that of the entropic term, so that the free energy change is largely negative with associated stability constants around 10^{50} and 10^{44} for M062X-D3 and BLYP-D3 functionals, respectively. Upon water solvation, the complexation free energy drops substantially as expected from the large solvation energy of the free bromide anion. Anyway, it still has high negative values with associated stability constants around 10^{10} and 10^{14} for M062X-D3 and BLYP-D3 functionals, respectively.

To further check whether the tweezer−Br^- complex remains stable in highly polar solvents, a first-principles MDS of the complex in water was carried out. A movie that shows the complete simulation is provided in the Supporting Information. Figure 4 shows snapshots of the simulation taken at three

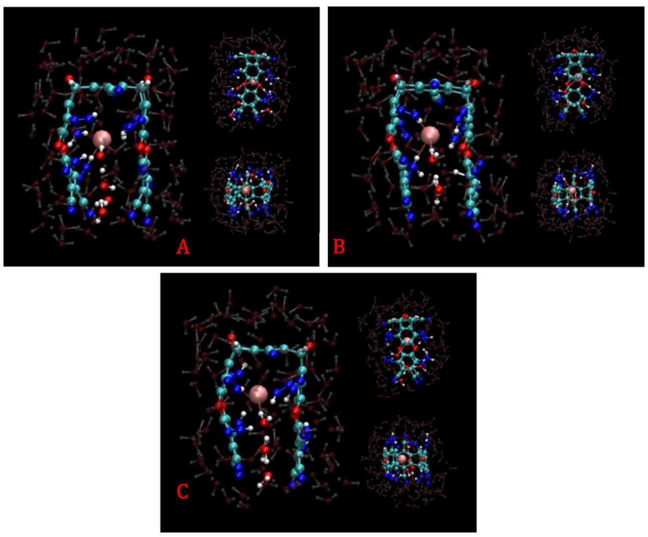

Figure 4. Snapshots of three different moments of the MD simulation, (A) at approximately 0 ps, (B) at approximately 5.5 ps, and (C) at approximately 11 ps.

different times of the MDS: at the beginning, middle, and at the end of the simulation. Despite three separate moments in time, there are several features that remain throughout the simulation and deserve attention: (1) there is always a water molecule inside the tweezer bonded to bromide by a hydrogen bond, (2) there are one or more azo substituents forming hydrogen bonds with the bromide ion, (3) there is a chain of water molecules within the tweezer' s cavity at the end of the two pincers and between them, and (4) bromide is always inside the tweezer near the center of the cavity. All of this can also be observed in the movie provided in the Supporting Information. The movie also shows the formation of hydronium and hydroxyl ions during the simulation due to proton transfer reactions between water molecules of the system.

We performed a structural analysis using the Travis package[46] to interpret quantitatively the observations mentioned above. Thus, we obtained from the simulation the distribution of the distance between bromide and the center of mass (C.M.) of the tweezer's frame. This distribution is shown in Figure 5. It shows that the most likely distance from bromide to the C.M. is about 40 pm and that most of the time

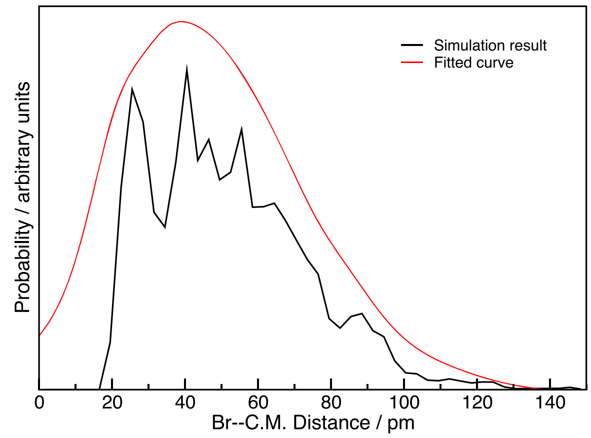

Figure 5. Bromide−C.M. distribution (see text).

bromide is between 25 and 60 pm away from the C.M. In fact, configurations with a distance larger than 80 pm are scarce. Additionally, we estimated that the distance from the C.M. to the border of the tweezer's cavity is always larger than 140 pm. Therefore, the bromide−tweezer complex is stable in water throughout the simulation since the anion remains inside the cavity trapped by the tweezer.

Figure 6 shows two radial distribution functions (RDFs), one is the RDF of bromide with the hydrogen atoms belonging to the azo groups (H_Twz) and the other is the pair correlation function of bromide and the rest of hydrogen atoms (H_no_Twz). In the latter RDF, we can see a sharp peak at 220 pm with a coordination number of 1 hydrogen atom at 270 pm. Considering the distance, it is likely that this peak appears due to the water molecule that is inside the tweezer's cavity. Furthermore, the narrow shape of the peak suggests a fairly fixed distance between the anion and the hydrogen atom, which agrees with a strong hydrogen bond between them. After the first peak, there is a zero-probability region, which means that there are no other water molecules forming hydrogen bonds with bromide. The RDF with H_Twz shows a broad peak between 240 and 280 pm and a valley at 365 pm that corresponds to a coordination number of 3 hydrogen atoms. Unlike the interaction with water, the broad peak implies weaker hydrogen bonds, but also, unlike water, bromide forms up to three hydrogen bonds with the azo groups, helping to keep the anion inside the tweezer's cavity.

With the results analyzed so far, we have seen that bromide establishes hydrogen bonds with one water molecule and with several azo groups. However, we do not know how often these hydrogen bonds appear simultaneously or whether the formation of a hydrogen bond between bromide and water prevents hydrogen bonds with the azo groups and vice versa. To evaluate the ability of bromide to establish simultaneously these kinds of hydrogen bonds, we presented a combination of two RDFs: the pair correlation function of bromide and the H_Twz hydrogens and the pair correlation function of bromide and the hydrogens of the water molecule inside the cavity (H_Wat). This representation is shown in Figure 7 using a 2D contour plot with a color scale to show how likely is the combination of two distances. The figure shows two vertical columns separated by a gap of approximately 80 pm, and each contour corresponds to a hydrogen of the water molecule. The shape of this figure matches a configuration in which a hydrogen atom from the water molecule always points

https://doi.org/10.1021/acs.jcim.1c00595
J. Chem. Inf. Model. 2021, 61, 4455−4461

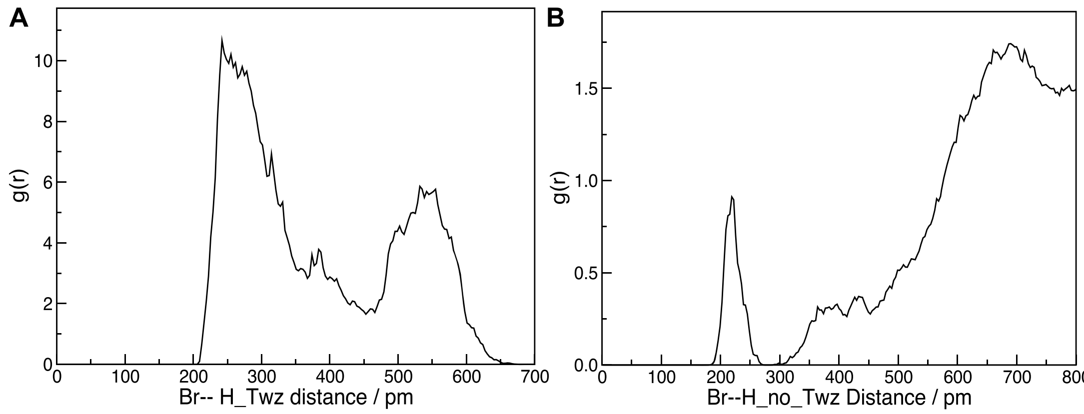

Figure 6. RDFs: (A) between bromide and the hydrogen atoms that belong to the azo groups (H_Twz) and (B) between bromide and those hydrogen atoms that do not belong to the azo groups (H_no_Twz).

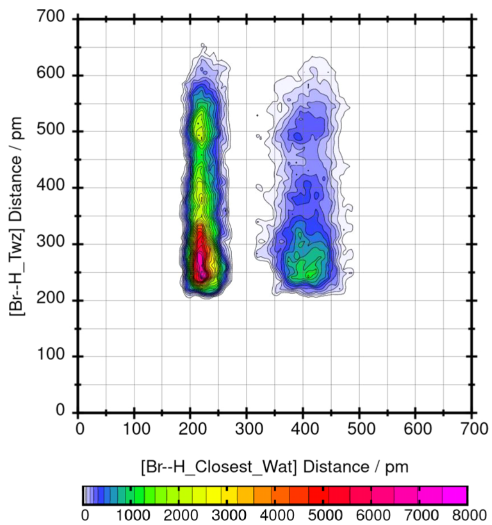

Figure 7. Two-dimensional histogram using the Br−H_Wat (see text) distance and the Br−H_Twz distance.

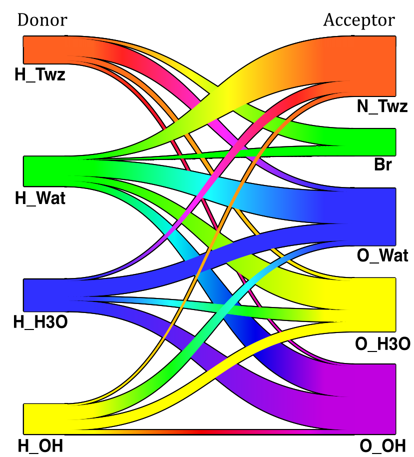

Figure 8. Hydrogen bonding topology of the system. H_Twz, H_Wat, H_H3O, and H_OH denote the hydrogen atoms of the azo groups, the water molecules, the hydronium cations, and the hydroxyl anions, respectively. N_Twz denotes the nitrogen atoms of the azo groups. Br denotes the bromide ion. O_Wat, O_H3O, and O_OH denote the oxygen atoms of the water molecules, the hydronium cations, and the hydroxyl anions, respectively.

at the bromide while the other points in the opposite direction. We can see how the maximum probability corresponds to configurations where the Br−H_Wat distance is between 200 and 220 pm and the Br−H_Twz distance is between 230 and 340 pm. This result indicates that the most likely configuration corresponds to geometries where both hydrogen bonds are formed simultaneously. The competition between water and the azo groups for bromide does not seem to destabilize the anion inside the tweezer's cavity. On the contrary, the combination of both interactions appears to keep it inside, protecting the anion from the influence of the external water molecules. 2D contour plots representing distances versus time are also provided in the Supporting Information (Figure S2). These graphs corroborate that the observations inferred from RDFs shown in Figures 6 and 7 are maintained throughout the simulation.

The hydrogen bonding topology of the system is illustrated in Figure 8, which displays the hydrogen bond donors on the left-hand side and the acceptors on the right-hand side. The width of the connection bars is proportional to the number of hydrogen bonds. Since hydronium and hydroxyl ions appear during the simulation due to proton transfer reactions, we also considered those species to analyze the ratio of hydrogen bonds in the system. The figure shows that bromide creates hydrogen bonds only with the azo groups and with water but not with the hydronium and hydroxyl ions. It can also be observed that the hydrogen atoms of the azo groups form hydrogen bonds mostly with the water oxygens, and that they form very few hydrogen bonds with the hydronium and the hydroxyl ions. All these observations indicate that the hydronium and the hydroxyl ions do not enter the tweezer's cavity. The figure shows that hydronium and hydroxyl ions not only form hydrogen bonds with each other but also with water, suggesting that proton transfer reactions involve the creation of large clusters that include one or more water molecules.

Finally, using a method described elsewhere,[46] we calculated the average lifetime of the different hydrogen bonds. We obtained lifetimes of 5.54 and 1.71 ps for the Br−H_Wat and Br−H_Twz hydrogen bonds, respectively. These lifetimes are long enough to indicate the well-established hydrogen bonds.

■ CONCLUSIONS

A neutral molecular tweezer merging aromatic and polar interaction centers is proposed as a highly efficient anion catcher in polar environments. Static and dynamic simulations, using a bromide anion in water as a model, have been carried out in order to evaluate the ability of the proposed tweezer to recognize anions. According to the DFT static calculations performed in this study, the anion−tweezer interaction energies are within the range of covalent or ionic bonds and the stability constants in water exceed 10 orders of magnitude due to the synergy between the aromatic−π and hydrogen bonding interactions. First-principles MDS corroborate the stability through the time of the anion−tweezer complex in water. It shows that the anion is effectively trapped within the tweezer's cavity, near its center. It also shows that a water molecule remains inside the cavity throughout the simulation, linked to the anion by a hydrogen bond. However, the formation of this hydrogen bond does not hinder the presence of the anion within the cavity but, on the contrary, it protects the anion from the influence of the external solvent environment, helping the anion to stay inside the tweezer's cavity. Thus, this computational work clearly shows that anion receptors based on neutral molecular tweezers can efficiently work in highly polar systems. The combination of azo groups and aromatic units in clip- or tweezer-like structures can serve as a guide for experimentalists to design potential receptors of anions with different chemical structures and sizes.

■ ASSOCIATED CONTENT

Supporting Information

The Supporting Information is available free of charge at https://pubs.acs.org/doi/10.1021/acs.jcim.1c00595.

Two-dimensional histogram of the distances between bromide and water hydrogens and between bromide and azo hydrogens, time-dependent distribution function of the distance between bromide and water hydrogens, and cartesian coordinates, energy, and frequencies of the complexes optimized at different computational levels (PDF)

Molecular dynamics simulation (MP4)

■ AUTHOR INFORMATION

Corresponding Author

Jose M. Hermida-Ramón − *Department of Physical Chemistry, Faculty of Chemistry, University of Vigo, 36310 Vigo, Galicia, Spain*; orcid.org/0000-0002-5354-2386; Email: jose_hermida@uvigo.es

Authors

Marta Queizán − *Department of Physical Chemistry, Faculty of Chemistry, University of Vigo, 36310 Vigo, Galicia, Spain*

Marta Sánchez-Lozano − *Department of Physical Chemistry, Faculty of Chemistry, University of Vigo, 36310 Vigo, Galicia, Spain*

Marcos Mandado − *Department of Physical Chemistry, Faculty of Chemistry, University of Vigo, 36310 Vigo, Galicia, Spain*; orcid.org/0000-0001-9688-2658

Complete contact information is available at: https://pubs.acs.org/10.1021/acs.jcim.1c00595

Notes

The authors declare no competing financial interest.

The program package used to perform the static calculations to obtain the minima in the gas phase is the commercial suite of programs: Gaussian 09 version D.01. Webpage: https://gaussian.com. An own software was used to perform the EDA (contact email mandado@uvigo.es). The dispersion correction component, DFT-D3, was obtained using the Grimme's free software. Webpage: https://www.chemie.uni-bonn.de/pctc/mulliken-center/software/dft-d3/. The topological analysis was carried out with the commercial package AIM2000. Webpage: http://aim2000.de. The freeware program package Orca v.4.2.1 was used to perform the MDS. Webpage: https://orcaforum.kofo.mpg.de/app.php/portal. The analysis of the molecular dynamics results was carried out with the Travis Open-source freeware. Webpage: http://www.travis-analyzer.de. Cartesian coordinates of the final structures (the minima) of the static calculations and the inputs for the equilibration and the production runs of the molecular dynamics calculations are provided in the Supporting Information.

■ ACKNOWLEDGMENTS

The authors thank Xunta de Galicia for financial support through the project GRC2019/24. M.Q. is also grateful to Xunta de Galicia for the award of a research grant.

■ REFERENCES

(1) Schneider, H.-J.; Yatsimirski, A. *Principles and Methods in Supramolecular Chemistry*: J. Wiley: New York, 2000.

(2) Mascal, M.; Armstrong, A.; Bartberger, M. D. Anion-aromatic bonding: a case for anion recognition by pi-acidic rings. *J. Am. Chem. Soc.* **2002**, *124*, 6274−6276.

(3) Quiñonero, D.; Garau, C.; Rotger, C.; Frontera, A.; Ballester, P.; Costa, A.; Deyà, P. M. Anion−π Interactions: Do They Exist? *Angew. Chem., Int. Ed.* **2002**, *41*, 3389−3392.

(4) Alkorta, I.; Rozas, I.; Elguero, J. Interaction of Anions with Perfluoro Aromatic Compounds. *J. Am. Chem. Soc.* **2002**, *124*, 8593−8598.

(5) Kim, D.; Tarakeshwar, P.; Kim, K. S. Theoretical Investigations of Anion−π Interactions: The Role of Anions and the Nature of π Systems. *J. Phys. Chem. A* **2004**, *108*, 1250−1258.

(6) Schottel, B. L.; Chifotides, H. T.; Dunbar, K. R. Anion−π Interactions. *Chem. Soc. Rev.* **2008**, *37*, 68−83.

(7) Berryman, O. B.; Johnson, D. W. Experimental evidence for interactions between anions and electron-deficient aromatic rings. *Chem. Commun.* **2009**, *22*, 3143−3153.

(8) Chifotides, H. T.; Dunbar, K. R. Anion−π Interactions in Supramolecular Architectures. *Acc. Chem. Res.* **2013**, *46*, 894−906.

(9) Frontera, A. Encapsulation of anions: Macrocyclic receptors based on metal coordination and anion−π interactions. *Coord. Chem. Rev.* **2013**, *257*, 1716−1727.

(10) Biedermann, F.; Schneider, H.-J. Experimental Binding Energies in Supramolecular Complexes. *Chem. Rev.* **2016**, *116*, 5216−5300.

(11) Molina, P.; Zapata, F.; Caballero, A. Anion Recognition Strategies Based on Combined Noncovalent Interactions. *Chem. Rev.* **2017**, *117*, 9907−9972.

(12) Kan, X.; Liu, H.; Pan, Q.; Li, Z.; Zhao, Y. Anion-π interactions: From concept to application. *Chin. Chem. Lett.* **2018**, *29*, 261−266.

(13) Tam, T. L. D.; Xu, J. W. The role of fluoride in anion−π interaction with naphthalene diimide. *Chem. Commun.* **2019**, *55*, 6225−6228.

(14) Rather, I. A.; Wagay, S. A.; Ali, R. Emergence of anion-π interactions: The land of opportunity in supramolecular chemistry and beyond. *Coord. Chem. Rev.* **2020**, *415*, No. 213327.

(15) Spichiger-Keller, U. S. *Chemical Sensors and Biosensors for Medical and Biological Applications*. Wiley-VCH: Weinheim, Germany, 1998.

(16) Mason, C. F. *Biology of Freshwater Pollution*, 2nd ed. Longman: New York, 1991.

(17) Bianchi, A.; Bowman-James, K.; Garcia-España, E. *Supramolecular Chemistry of Anions*. Wiley-VCH: New York, 1997.

(18) Langton, M. J.; Serpell, C. J.; Beer, P. D. Anion Recognition in Water: Recent Advances from a Supramolecular and Macromolecular Perspective. *Angew. Chem., Int. Ed.* **2016**, *55*, 1974−1987.

(19) Wang, D.-X.; Wang, M.-X. Exploring Anion−π Interactions and Their Applications in Supramolecular Chemistry. *Acc. Chem. Res.* **2020**, *53*, 1364−1380.

(20) Klärner, F. G.; Benkhoff, J.; Boese, R.; Burkert, U.; Kamieth, M.; Naatz, U. Molecular Tweezers as Synthetic Receptors in Host—Guest Chemistry: Inclusion of Cyclohexane and Self-Assembly of Aliphatic Side Chains. *Angew. Chem., Int. Ed.* **1996**, *35*, 1130−1133.

(21) Klärner, F.-G.; Burkert, U.; Kamieth, M.; Boese, R.; Benet-Buchholz, J. Molecular Tweezers as Synthetic Receptors: Molecular Recognition of Electron-Deficient Aromatic and Aliphatic Substrates. *Chem.−Eur. J.* **1999**, *5*, 1700−1707.

(22) Klärner, F.-G.; Kahlert, B. Molecular Tweezers and Clips as Synthetic Receptors. Molecular Recognition and Dynamics in Receptor−Substrate Complexes. *Acc. Chem. Res.* **2003**, *36*, 919−932.

(23) Lobert, M.; Bandmann, H.; Burkert, U.; Büchele, U. P.; Podsadlowski, V.; Klärner, F.-G. Dynamics in Host−Guest Complexes of Molecular Tweezers and Clips. *Chem.−Eur. J.* **2006**, *12*, 1629−1641.

(24) Hermida-Ramón, J. M.; Estévez, C. M. Towards the Design of Neutral Molecular Tweezers for Anion Recognition. *Chem.−Eur. J.* **2007**, *13*, 4743−4749.

(25) Hermida-Ramón, J. M.; Mandado, M.; Sánchez-Lozano, M.; Estévez, C. M. Enhancing the interactions between neutral molecular tweezers and anions. *Phys. Chem. Chem. Phys.* **2010**, *12*, 164−169.

(26) Sánchez-Lozano, M.; Otero, N.; Hermida-Ramón, J. M.; Estévez, C. M.; Mandado, M. Anion-π Aromatic Neutral Tweezers Complexes: Are They Stable in Polar Solvents? *J. Phys. Chem. A* **2011**, *115*, 2016−2025.

(27) Etzkorn, M.; Timmerman, J. C.; Brooker, M. D.; Yu, X.; Gerken, M. Preparation, structures and preliminary host−guest studies of fluorinated syn-bis-quinoxaline molecular tweezers. *Beilstein J. Org. Chem.* **2010**, *6*, 39.

(28) Berryman, O. B.; Sather, A. C.; Hay, B. P.; Meisner, J. S.; Johnson, D. W. Solution Phase Measurement of Both Weak σ and C−H···X−Hydrogen Bonding Interactions in Synthetic Anion Receptors. *J. Am. Chem. Soc.* **2008**, *130*, 10895−10897.

(29) Liu, Y.-Z.; Lv, L.-L.; Li, H.-X.; Li, Z.-F.; Yuan, K. A theoretical insight into several common anion recognitions based on double-dentate hydrogen bond and anion-π coexistence. *J. Phys. Org. Chem.* **2019**, *32*, No. e3959.

(30) Savastano, M.; Bazzicalupi, C.; García-Gallarín, C.; López de la Torre, M. D.; Bianchi, A.; Melguizo, M. Supramolecular forces and their interplay in stabilizing complexes of organic anions: tuning binding selectivity in water. *Org. Chem. Front.* **2019**, *6*, 75−86.

(31) de Bettencourt-Dias, A.; Beeler, R. M.; Zimmerman, J. R. Anion-π and H-Bonding Interactions Supporting Encapsulation of $[Ln(NO_3)_{6/5}]^{3-/2-}$ (Ln = Nd, Er) with a Triazine-Based Ligand. *J. Am. Chem. Soc.* **2019**, *141*, 15102−15110.

(32) Grimme, S.; Antony, J.; Ehrlich, S.; Krieg, H. A consistent and accurate ab initio parametrization of density functional dispersion correction (DFT-D) for the 94 elements H-Pu. *J. Chem. Phys.* **2010**, *132*, 154104.

(33) Burns, L. A.; Mayagoitia, Á. V.; Sumpter, B. G.; Sherrill, C. D. Density-functional approaches to noncovalent interactions: a comparison of dispersion corrections (DFT-D), exchange-hole dipole moment (XDM) theory, and specialized functionals. *J. Chem. Phys.* **2011**, *134*, No. 084107.

(34) Ramos-Berdullas, N.; Pérez-Juste, I.; Van Alsenoy, C.; Mandado, M. Theoretical study of the adsorption of aromatic units on carbon allotropes including explicit (empirical) DFT dispersion corrections and implicitly dispersion-corrected functionals: the pyridine case. *Phys. Chem. Chem. Phys.* **2015**, *17*, 575−587.

(35) Frisch, M. J.; Trucks, G. W.; Schlegel, H. B.; Scuseria, G. E.; Robb, M. A.; Cheeseman, J. R.; Scalmani, G.; Barone, V.; Petersson, G. A.; Nakatsuji, H. *Gaussian 09*. Gaussian, Inc.: Wallingford, CT, 2009.

(36) Neese, F. The ORCA program system. *WIREs Comput. Mol. Sci.* **2012**, *2*, 73−78.

(37) Neese, F. Software update: the ORCA program system, version 4.0. *WIREs Comput. Mol. Sci.* **2018**, *8*, No. e1327.

(38) Mandado, M.; Hermida-Ramón, J. M. Electron Density Based Partitioning Scheme of Interaction Energies. *J. Chem. Theory Comput.* **2011**, *7*, 633−641.

(39) Boys, S. F.; Bernardi, F. The calculation of small molecular interactions by the differences of separate total energies. Some procedures with reduced errors. *Mol. Phys.* **1970**, *19*, 553−566.

(40) Bader, R. F. W. *Atoms in Molecules - A Quantum Theory*. Oxford University Press: Oxford, UK, 1990.

(41) AIM 2000. Version 2.0, Program designed by Friedrich Biegler-König and Jens Schönbohm, 2002.

(42) Berendsen, H. J. C.; Postma, J. P. M.; van Gunsteren, W. F.; DiNola, A.; Haak, J. R. Molecular dynamics with coupling to an external bath. *J. Chem. Phys.* **1984**, *81*, 3684−3690.

(43) Slipchenko, L. V.; Gordon, M. S.; Ruedenberg, K. Dispersion Interactions in QM/EFP. *J. Phys. Chem. A* **2017**, *121*, 9495−9507.

(44) de Azevedo Santos, L.; Ramalho, T. C.; Hamlin, T. A.; Bickelhaupt, F. M. Chalcogen bonds: Hierarchical ab initio benchmark and density functional theory performance study. *J. Comput. Chem.* **2021**, *42*, 688−698.

(45) Marenich, A. V.; Cramer, C. J.; Truhlar, D. G. Universal Solvation Model Based on Solute Electron Density and on a Continuum Model of the Solvent Defined by the Bulk Dielectric Constant and Atomic Surface Tensions. *J. Phys. Chem. B* **2009**, *113*, 6378−6396.

(46) Brehm, M.; Thomas, M.; Gehrke, S.; Kirchner, B. TRAVIS—A free analyzer for trajectories from molecular simulation. *J. Chem. Phys.* **2020**, *152*, 164105−164120.

https://doi.org/10.1021/acs.jcim.1c00595
J. Chem. Inf. Model. 2021, 61, 4455−4461